International Journal of Radiation Biology, April 2015; 91(4): 329–335

ISSN 0955-3002 print / ISSN 1362-3095 online
DOI: 10.3109/09553002.2014.995381

informa
healthcare

Neutron autoradiography to study boron compound microdistribution in an oral cancer model

Agustina Portu[1,2], Ana Julia Molinari[1,2], Silvia Inés Thorp[1], Emiliano César Cayetano Pozzi[1], Paula Curotto[1], Amanda Elena Schwint[1,2] & Gisela Saint Martin[1]

[1]*National Atomic Energy Commission (CNEA), San Martin, Buenos Aires, Argentina, and* [2]*National Council of Scientific and Technological Research (CONICET), Ciudad Autónoma de Buenos Aires, Argentina*

Abstract

Purpose: **We previously reported the therapeutic efficacy of Sequential Boron Neutron Capture Therapy (Seq-BNCT), i.e., BPA (boronophenylalanine) – BNCT followed by GB-10 (decahydrodecaborate) – BNCT 1 or 2 days later, in the hamster cheek pouch oral cancer model. We have utilized the neutron autoradiography methodology to study boron microdistribution in tissue. The aim was to use this method to evaluate if the distribution of GB-10 is altered by prior application of BPA-BNCT in Sequential BNCT protocols.**

Materials and methods: **Extensive qualitative and quantitative autoradiography analyses were performed in the following groups: G1 (animals without boron); G2 (animals injected with BPA); G3 (animals injected with GB-10); G4 (same as G3, 24 h after BPA-BNCT); and G5 (same protocol as G4, 48 h interval).**

Results: **A detailed study of boron localization in the different tissue structures of tumor, premalignant and normal tissue in the hamster cheek pouch was performed. GB-10 accumulated preferentially in non-neoplastic connective tissue, whereas for BPA neoplastic cells showed the highest boron concentration. Boron distribution was less heterogeneous for GB-10 than for BPA. In premalignant and normal tissue, GB-10 and BPA accumulated mostly in connective tissue and epithelium, respectively.**

Conclusions: **BPA-BNCT could alter boron microlocalization of GB-10 administered subsequently. Boron targeting homogeneity is essential for therapeutic success.**

Keywords: Neutron autoradiography, boron microdistribution, Sequential BNCT, GB-10, BPA, oral cancer

Introduction

When a heavy ion passes through a Solid State Nuclear Track Detector (SSTND), a damaged zone along the particle path is permanently created in the detector. This latent track can be amplified up to light microscopy level by an appropriate chemical treatment, as the etching velocity in the damaged zone is higher than the velocity in the non irradiated material (bulk velocity). In particular, if a tissue section that contains a heavy particle emitter is placed in contact with a SSNTD, the track density analysis on the detector enables the determination of the spatial distribution of the element in the sample (Fleischer et al. 1975). The charged particles can originate from the natural decay of unstable isotopes or be the result of a nuclear reaction of a target with neutrons (i.e., neutron capture radiography).

Boron Neutron Capture Therapy (BNCT) is based on the nuclear reaction that occurs when the stable isotope ^{10}B is exposed to a thermal neutron flux, producing high linear energy transfer alpha particles and lithium recoils. The He and Li ions are ejected in opposite directions and deposit their energy in a short range (about the diameter of one cell). If large amounts of boron are targeted to tumor cells, they would receive a lethal radiation dose, preserving surrounding normal tissue (Barth et al. 2012). In this way, the successful application of BNCT strongly depends on the intratumoural delivery of ^{10}B. Within this context, a boron determination method that provides information about differences in boron uptake and distribution would be very useful. The analysis of the autoradiography images formed from the individual tracks of the alpha and lithium particles provides information on the spatial distribution of boron in tissues (e.g., Yanagie et al. 2004, Altieri et al. 2006, Schütz et al. 2011). These data can be used for localized dosimetric evaluation (Lu and Kiger 2009). We have enhanced the resolution of conventional neutron autoradiography by using the same tissue section for both broad histological study and generation of an autoradiographic image (Portu et al. 2013). This modification improves resolution without resorting to the use of thin detectors as in the technically complex technique of High Resolution Quantitative Autoradiography (HRQAR) (Solares and Zamenhof 1995, Kiger et al. 2002).

Two boron compounds have been used clinically: Boronophenylalanine (BPA) and sodium mercaptoundecahydro-*closo*-dodecaborate (BSH) (Coderre et al. 2003). Sodium decahydrodecaborate (GB-10) is also currently authorized

Correspondence: Dr Agustina Mariana Portu, Department of Radiobiology, National Atomic Energy Commission (CNEA), Av. General Paz 1499, B1650KNA, San Martin, Buenos Aires, Argentina. Tel: + 54 11 6772 7933/7150. E-mail: agustina.portu@gmail.com/portu@cnea.gov.ar.

(Received 26 March 2014; revised 12 November 2014; accepted 25 November 2014)

for use in human beings by the Food and Drug Administration (FDA, USA) as IND (Investigational New Drug) (Hawthorne and Lee 2003) although it was used clinically only for two cases (Sweet et al. 1963, Asbury et al. 1972) and in a pharmacological study in humans (Diaz et al. 2002). Gross concentration of ^{10}B in tissue samples can be obtained by analytical methods, such as inductively coupled plasma-optical emission spectroscopy/mass spectrometry (ICP-OES/ICP-MS) (Wittig et al. 2008). In recent studies, variations in tumor response have been reported between BNCT protocols, although similar absolute gross boron concentration values in tumor were measured (Molinari et al. 2012). Thus, divergence in gross boron concentration is not enough to explain differences in therapeutic response.

In a previous study we demonstrated the therapeutic success of Sequential BNCT in the hamster cheek pouch oral cancer model (Molinari et al. 2011). This protocol involves a sequential application of BPA-BNCT followed by GB-10-BNCT with an interval of 24 or 48 h between the two treatments. The first application of BPA-BNCT could conceivably alter GB-10 biodistribution for the second application. However, no significant changes were detected in terms of gross boron content measured ICP-MS and ICP-OES. Throughout this report, we define macrodistribution of boron as the ^{10}B concentration value obtained with gross boron determination techniques (such as ICP-OES or ICP-MS), whereas microdistribution of boron is defined as the spatially localized boron content in the different regions of the tissue structure. The analysis of boron microdistribution can be performed both qualitatively (by the analysis of high track density images) and quantitatively (if knowledge of the absolute ^{10}B concentration in the different tissue regions is required).

Within this context, the aim of the present study was to explore potential changes in boron microdistribution that are not detectable by gross boron measurements, using the neutron capture autoradiography imaging capability, in order to evaluate if the distribution of GB-10 is altered by prior application of BPA-BNCT in Sequential BNCT protocols. Tumor microdistribution of ^{10}B delivered by GB-10 was evaluated and compared with tumor microdistribution of BPA. For the first time, a detailed study of the boron uptake was performed at tissue level in the different regions of tumor, premalignant and normal tissue in the hamster cheek pouch oral cancer model.

Materials and methods

Six-week old female/male syrian hamsters (weight range: 90–200 g, supplied by the animal breeding facility of the National Atomic Energy Commission, Ezeiza, Argentina) were fed an *ad libitum* standard chow diet (Cooperación, Buenos Aires, Argentina) and were submitted to a previously described carcinogenesis protocol (e.g., Molinari et al. 2012). Institutional guidelines for the care and use of laboratory animals were strictly followed. The samples for the autoradiographic analysis were obtained from five experimental groups of tumor-bearing hamsters. (i) G1 (control): not irradiated, no boron compound injection. (ii) G2 (BPA): animals injected with BPA (Interpharma, Praha, Czech Republic) at a dose of 15.5 mg ^{10}B/kg body weight (bw) and euthanized 3 h post administration of BPA. (iii) G3 (GB-10): animals injected with GB-10 (Neutron Therapies L.L.C., San Diego, CA, USA) at a dose of 50 mg ^{10}B/kg bw and euthanized 3 h post administration of GB-10. (iv) G4 (GB10 24 h post BPA-BNCT): animals treated with BNCT mediated by BPA. After 24 h, they were injected with GB-10 at the same dose as G3 and euthanized 3 h post administration of GB-10. (v) G5 (GB10 48 h post BPA-BNCT): the same protocol as G4, but the injection of GB-10 was performed 48 h after BPA-BNCT. The doses for BPA and GB-10 were chosen according to previous biodistribution studies (e.g., Kreimann et al. 2001, Heber et al. 2004).

For G4 and G5, the BPA-BNCT irradiations were performed at the neutron source constructed for use in BNCT biomedical applications by the National Atomic Energy Commission of Argentina at the RA-3 (Reactor Argentino 3) research and production nuclear reactor facility (Ezeiza, Buenos Aires, Argentina), as previously described (Molinari et al. 2011). The total absorbed dose prescribed to tumor in both cases was 4 ± 1 Gy. The effective irradiation time was 3.13 min for G2, G4 and G5 and 4.96 min for G3 (Molinari et al. 2011). All hamsters were euthanized 3 h post administration of GB-10 or BPA, as previous biodistribution studies demonstrated that the maximum boron concentration value is reached between 3 and 3.5 h. These biodistribution studies also showed that the boron concentration in blood and tissues 24 h after the administration of BPA was negligible (Kreimann et al. 2001, Heber et al. 2004, 2006). Thus BPA was considered not to contribute to boron levels after administration of GB-10 in the 'Sequential' protocols (Molinari et al. 2011).

Samples of tumor, premalignant and normal pouch tissue were excised and fixed with liquid nitrogen. All samples were sectioned at 30 μm in a cryostatic microtome (CM 1850 Leica Microsystems, Heidelberg, Baden-Wurtemberg, Germany) and mounted on polycarbonate nuclear track detector foils (Lexan™, SABIC Innovative Plastics, Pittsfield, MA, USA).

In addition to a qualitative analysis (QLA), a quantitative evaluation (quantitative analysis, QTA) was performed to obtain an absolute boron concentration value for each region of the tissue, by evaluating track density in the corresponding regions of the detector as previously described (Portu et al. 2011a). Depending on the type of analysis to be performed, the assemblies were exposed to one of the following thermal neutrons fluences at the RA-3 nuclear reactor: 10^{12} n cm^{-2} for QTA and 10^{13} n cm^{-2} for QLA. QLA samples were explored and processed as described in Portu et al. (2013). QTA foils were marked with reference points and stained with haematoxylin-eosin (H&E, Biopur, Rosario, Santa Fe, Argentina). By microscopic examination, regions of the tumor (neoplastic cells [NC] and non-neoplastic connective tissue [NNC]) and of premalignant and normal tissue (epithelium [E]; loose connective tissue [C], and muscle [M]) were delimited using an x-y grid defined using the points of reference. Then, tissue was removed with a trypsine-EDTA (ethylenediaminetetraacetic acid disodium salt dihydrate) solution (Sigma Life Science, St. Louis, MO, USA) and the foils were chemically

etched with PEW (Potassium hydroxide + Ethanol + Water) solution (30 g KOH [Mallinckrodt, New York, USA] + 80 g ethyl alcohol [Merck, Darmstadt, Hesse, Germany] + 90 g distilled water) at 70°C. QTA samples were etched during 2 min, whereas an etching time of 6 min was established for QLA samples. Each of the previously delimited areas was re-accessed employing the points of reference and a motorized microscope stage. The lateral resolution is ≤ 10 μm. Track density was measured for each zone in QTA foils and then converted to ^{10}B concentration values using a calibration system developed in our laboratory (Portu et al. 2011b). Also, an overall value was obtained by counting 50 fields per foil. The determination limit in boron concentration is around 1 ppm. Three slices per sample were analyzed to obtain a mean value per animal. Data from four animals were averaged per protocol. These results were compared with boron content of the leftover tissue measured by ICP-MS (ELAN® DRC II, Perkin Elmer, Waltham, MA, USA).

The following ratio was defined as an indicator of boron targeting homogeneity in tumor:

$$\frac{\text{NNC}}{\text{NC}} = \frac{\text{Boron concentration in non} - \text{neoplastic connective tissue}}{\text{Boron concentration in neoplastic cells}} \quad (1)$$

A ratio of 1 indicates the highest grade of homogeneity.

The quantitative results are presented as mean value ± standard deviation (SD). The statistical significance was evaluated by Student's *t*-test, setting $p = 0.05$ as the threshold for statistical significance. The statistical analysis was confirmed by calculating a 95% confidence interval for the differences between means of unpaired samples.

Results

Examples of QLA (histology and autoradiography) corresponding to protocols G2 and G3 for tumor and G2 and G5 for premalignant tissue samples are shown in Figure 1 and 2, respectively. The boron pattern of normal pouch tissue samples was similar to that of premalignant tissue.

G1 (control group) autoradiographies (not shown) showed a small number of tracks, indicating the absence of boron contamination during the manipulation of the sample. Nevertheless, they were quantified in order to obtain the background contribution, which was within the uncertainty of the method (10%): (0.8 ± 0.4) ppm for tumor, (1 ± 2) ppm for premalignant tissue and (1 ± 1) ppm for normal pouch tissue.

The autoradiography images of the boron-containing groups (G2, G3, G4 and G5) presented higher track density values. Tracks were distributed heterogeneously, matching the diverse histological structures. This finding was revealed in the QLA images as variations in shades of grey, providing a rapid way to infer differences in boron uptake. The images

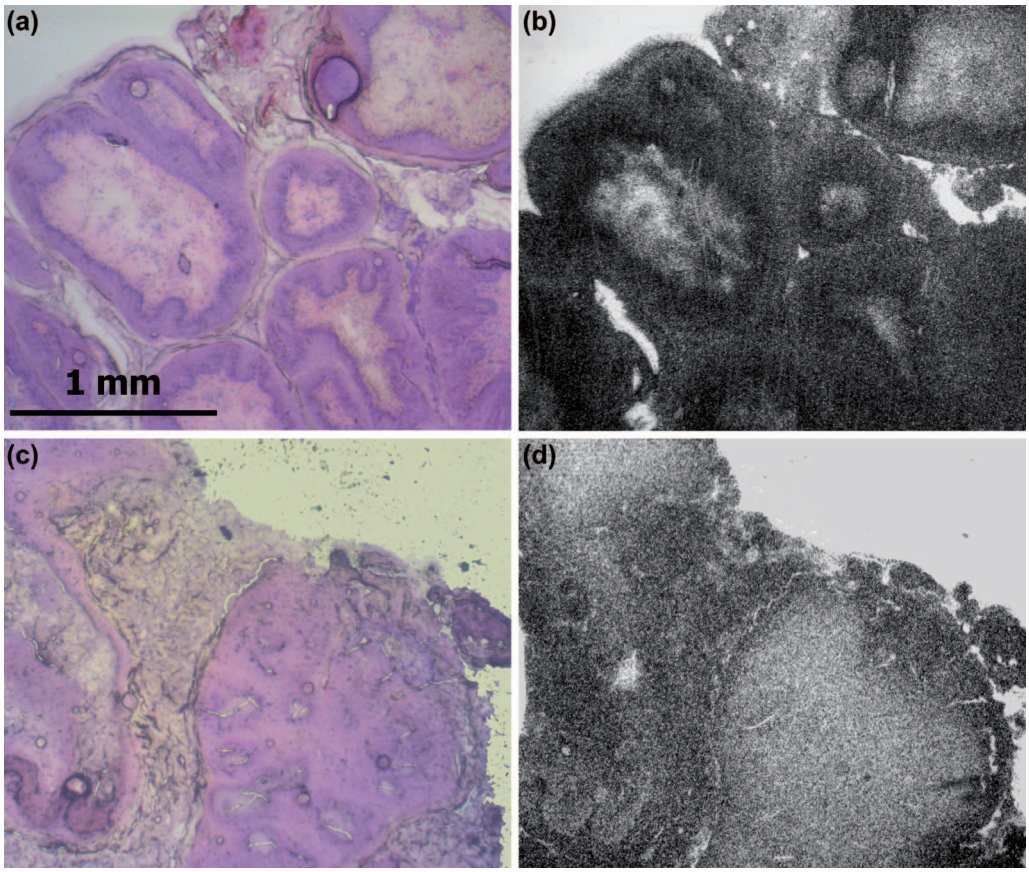

Figure 1. Haematoxylin-eosin stained tumor sections mounted on Lexan for (a) G2 (BPA) and (c) G3 (GB-10). (b) and (d) are the corresponding qualitative autoradiographic images of (a) and (c), respectively (2.5×). G2: animals injected with BPA (15.5 mg ^{10}B/kg bw). G3: animals injected with GB-10 (50 mg ^{10}B/kg bw). The scale is indicated in the top panel. This Figure is reproduced in color in the online version of *International Journal of Radiation Biology*.

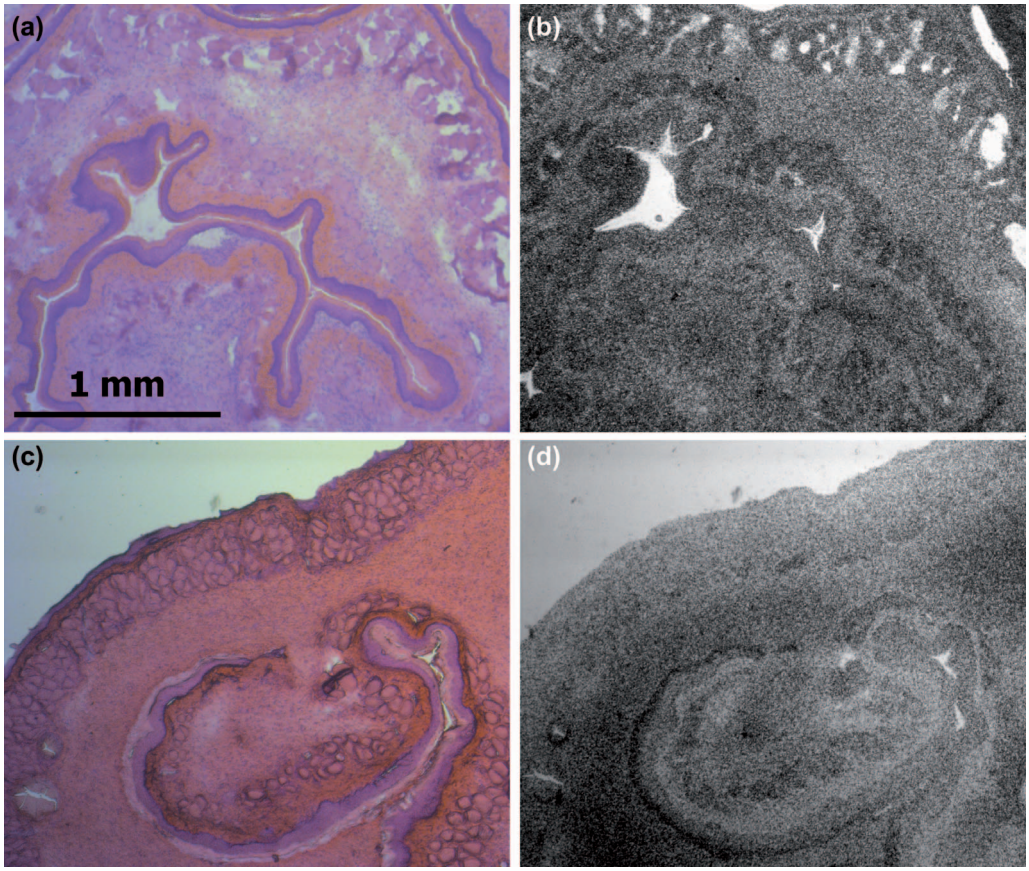

Figure 2. Haematoxylin-eosin stained premalignant tissue sections mounted on Lexan for (a) G2 (BPA) and (c) G5 (GB10 48 h post BPA-BNCT). (b) and (d) are the corresponding qualitative autoradiographic images of (a) and (c), respectively (2.5×) . G2: animals injected with BPA (15.5 mg ^{10}B/kg bw). G5 animals treated with BPA-BNCT followed by the injection of GB-10 (50 mg ^{10}B/kg bw, 48 h post irradiation). The scale is indicated in the top panel. This Figure is reproduced in color in the online version of *International Journal of Radiation Biology*.

also revealed irregularities produced in the cutting process. G3, G4 and G5 showed the same pattern of heterogeneity.

The histological images made it possible to outline areas within a single section, contributing to the evaluation of spatial distribution. It was possible to identify the different tissue structures on the autoradiographic images. Figure 3 shows some examples of G2 and G3 tumors at a higher magnification (20×). In tumor, BPA accumulated preferentially in neoplastic cells. Conversely, in G3, boron concentration in non-neoplastic connective tissue was higher than in neoplastic cells for GB-10. However, the heterogeneity observed for GB-10 seemed to be lower than for BPA. G4 and G5 samples showed the same pattern as G3.

The same analysis was performed for premalignant and normal pouch tissue. As shown in Figure 2, ^{10}B accumulated preferentially in epithelium for BPA whereas the highest concentration areas corresponded to connective tissue in the case of GB-10. In Figure 4, an example of G5 is presented at a higher magnification (10×). As observed for tumors, G3 and G4 samples showed the same pattern as G5.

QTA analysis for the boron-containing groups is summarized in the bar graphs presented in Figure 5 for tumor, premalignant and normal pouch tissue.

Standard deviations were large due to the biological variation between animals. No statistical differences were observed with ICP-MS measurements when considering mean values for each protocol, except for G5 tumor ($p = 0.0186$) and premalignant tissue ($p = 0.0364$) data. Moreover, by calculating 95% confidence intervals, except for G5 tumor, it can be inferred that there was no difference between means. The higher values of ^{10}B concentration correspond to G2 for all samples, whereas G3, G4 and G5 show similar global values. The heterogeneity found in QLA images for all protocols was confirmed. The NNC/NC ratio was 0.5 ± 0.1 for G2, while it was 1.4 ± 0.1 for G3 and G5 and 1.2 ± 0.2 for G4. For premalignant and normal tissue, the boron concentration values were higher in epithelium than in connective tissue and muscle in G2, whereas in the case of G3, G4 and G5 the values in connective tissue were higher than in muscle and epithelium. Overall boron concentration values in premalignant and normal tissue were similar for all protocols. In summary, the values for normal tissue were lower than their premalignant tissue counterparts. GB-10 accumulated preferentially in connective tissue whereas BPA uptake was higher in epithelium.

Discussion

The microdistribution of boron from GB-10 in tumor was assessed for the first time and compared with the microdistribution pattern of boron from BPA in tumor. Furthermore, the localization of boron from BPA and GB-10 in

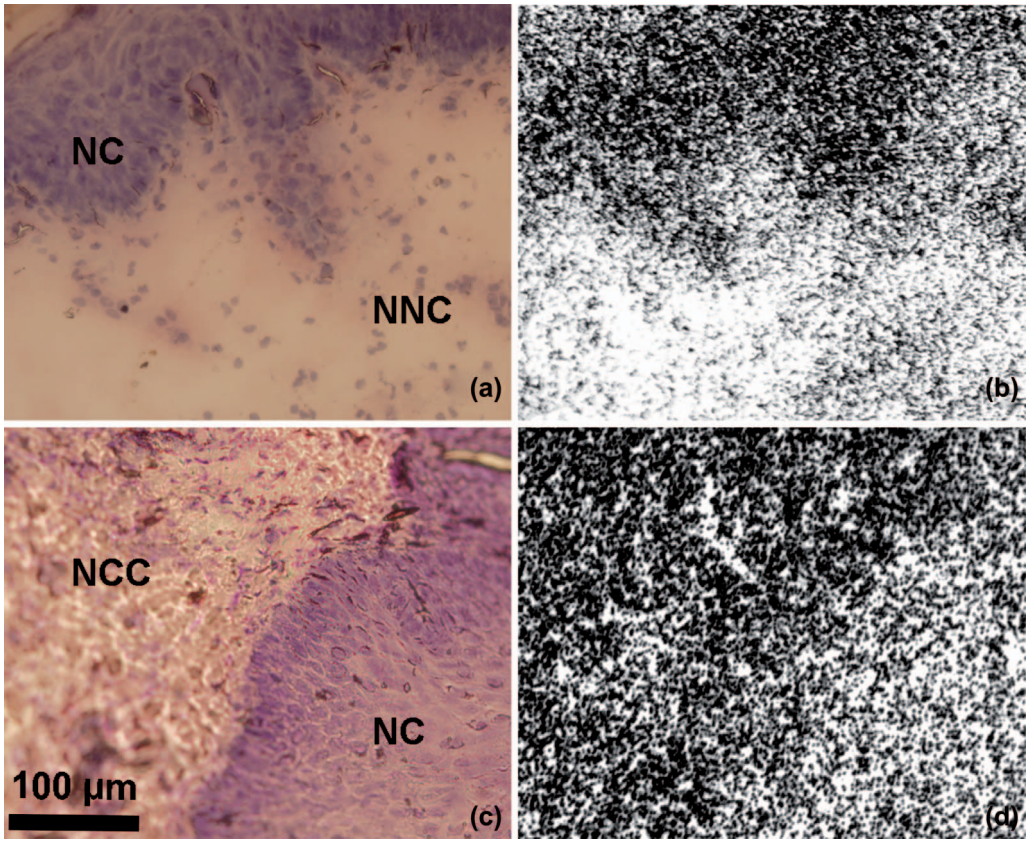

Figure 3. Haematoxylin-eosin stained tumor sections mounted on Lexan for (a) G2 (BPA) and (c) G3 (GB-10). (b) and (d) are the qualitative autoradiographic images of (a) and (c), respectively. NC, neoplastic cells; NCC, non-neoplastic connective tissue. Original magnification: 20×. This Figure is reproduced in color in the online version of *International Journal of Radiation Biology*.

premalignant and normal pouch tissue was determined. The microdistribution of boron in tumor, premalignant tissue and normal tissue was evaluated for different protocols to examine potential differences between boron compounds and tissues, and to assess the potential influence of BNCT on subsequent boron compound uptake and distribution. The autoradiographies obtained under the stated conditions reveal the histological map of the tissue sections, showing differences in boron uptake between areas. In a previous analysis of these compounds with gross boron measurement techniques (Heber et al. 2006), we reported that GB-10 is homogeneously targeted to tumor. These new results confirm that indeed GB-10 distribution is more homogeneous than BPA, as previously observed in Bortolussi et al. (2010), but is non-specific for neoplastic cells for all GB-10 protocols.

The heterogeneity observed in boron concentration for tumors would be in accordance with the high blood boron values previously reported for GB-10 (Trivillin et al. 2006), coupled to leakage from aberrant tumor blood vessels (Jain 2005). Given that GB-10 would enter cells by passive transport (e.g., Heber et al. 2004), it would not accumulate

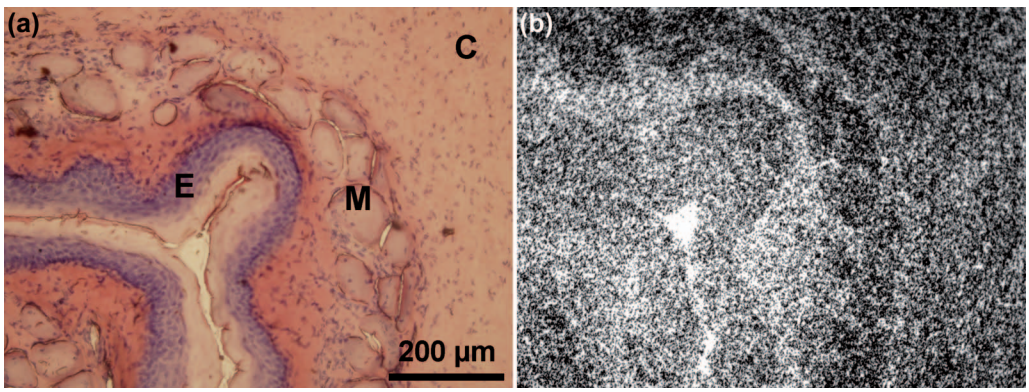

Figure 4. (a) Haematoxylin-eosin stained premalignant tissue section mounted on Lexan for G5 (GB-10 48 h post BPA-BNCT) and (b) its qualitative autoradiographic image. E, epithelium; M, muscle; C, connective tissue. Magnification: 10×. This Figure is reproduced in color in the online version of *International Journal of Radiation Biology*.

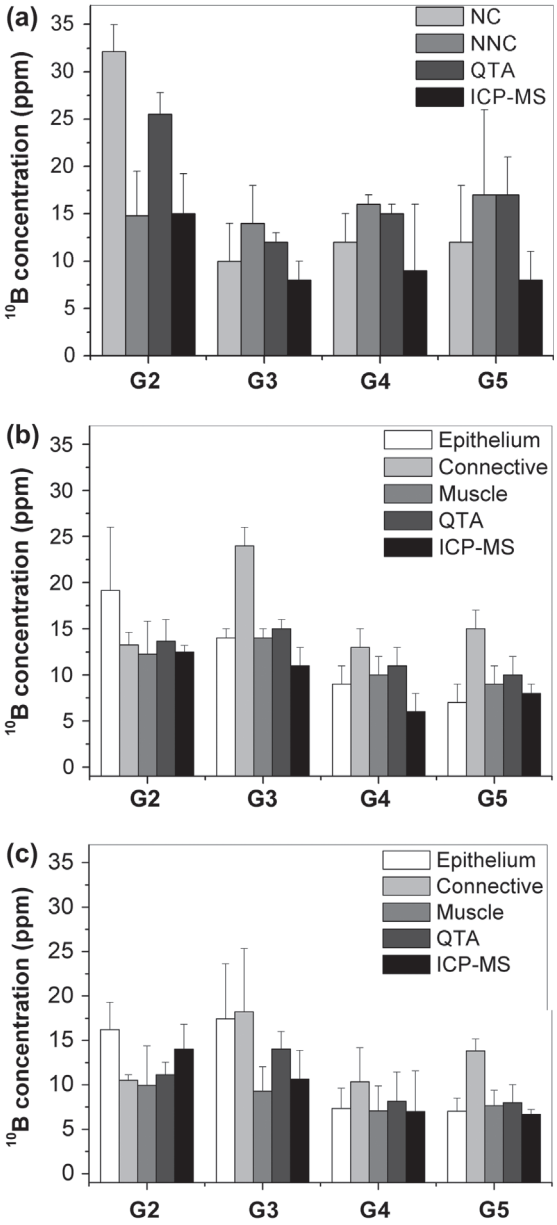

Figure 5. ICP-MS and QTA boron concentration values for (a) tumor, (b) premalignant tissue and (c) normal tissue, and for their corresponding histological areas (neoplastic cells [NC], non-neoplastic connective tissue [NNC], epithelium, connective tissue and muscle) for each of the boron protocols. Error bars indicate the standard deviation.

preferentially in neoplastic cells. BPA distribution would be more heterogeneous than GB-10 distribution, conceivably due to BPA active transport mechanisms (Wittig et al. 2000) that would allow for preferential targeting of neoplastic cells. Indeed, QTA boron concentration value for non-neoplastic connective tissue was almost 30% higher than for neoplastic cells in the case of GB-10. For BPA, boron concentration in non-neoplastic connective tissue concentration was 50% of the value in neoplastic cells. These results support our initial hypothesis that the therapeutic efficacy of 'Sequential' BNCT would stem from the use of two boron agents with different properties and complementary mechanisms of action, conceivably contributing to a more homogeneous, therapeutically successful targeting of heterogeneous tumor cells' populations. BPA-BNCT would target neoplastic cells, while GB-10 or BSH-BNCT would target the aberrant tumor vasculature. The sequential administration of the two applications would favor targeting with GB-10, as the IFP (interstitial fluid pressure) is reduced after BPA-BNCT.

QTA analysis also showed slight variations between G4 (GB10 24 h post BPA-BNCT) and G3 (GB10) and G5 (GB10 48 h post BPA-BNCT). The NNC/NC ratio closest to 1 was observed for G4, indicating more homogeneous tumor boron targeting. Although the difference in NNC/NC ratio between Seq 24 h (1.2 ± 0.2) and Seq 48 h (1.4 ± 0.1) would be marginal, this slight improvement in tumor boron targeting homogeneity would be associated to a slightly enhanced tumor response in animals treated with Seq-24h-BNCT compared to animals treated with Seq-48h-BNCT ($95 \pm 2\%$ vs. $91 \pm 3\%$) (Molinari et al. 2011).

For all groups, the global QTA boron concentration value fell within the range of values corresponding to each histological area (NC and NNC for tumor, E, C and M for premalignant and normal tissue), confirming the concept of overall measurement.

All the tissue structures that were identifiable at a histological level were analyzed qualitatively and quantitatively, with exception of the connective tissue underlying the epithelium in premalignant and normal pouch tissue sections (Figure 3). In the QLA images this area appeared lighter, regardless of the boron compound employed. However, we were unable to delineate the area reproducibly for evaluation. In this study we have brought the neutron autoradiography technique to the limit of its resolution. The assessment of small structures that cannot be photographed individually would require the use of high resolution techniques. An attractive option for this type of analysis is the use of tissue imprints following sensitization of the detector with ultraviolet radiation (UV-C, 254 nm) (Amemiya et al. 2005). Moreover, if cellular or subcellular accumulation of the compound were to be studied, quantitative secondary ion mass spectrometry is uniquely suited for microlocalization studies (Chandra et al. 2013, 2014).

We can conclude that non-selective accumulation occurs in different tissue areas for GB-10 and BPA in tumor, premalignant and normal tissue. Furthermore, the different boron compound administration protocols lead to different microdistribution patterns. The application of Sequential BNCT with a 24 h interval enhances GB-10 boron targeting homogeneity and favors tumor control. This finding confers on boron targeting homogeneity a pivotal role in therapeutic success. QLA images reproduced the histological structures with high quality, while QTA allowed for extensive and comprehensive evaluation of boron uptake to yield an indicator of targeting homogeneity. The technique proved successful to assess the spatial distribution of boron at a micrometer level resolution, with low cost in terms of time and complexity. Within this context, autoradiographic analysis provides information on the boron distribution/concentration that can be used to evaluate the localized dosimetry and interpret the radiobiological effects. This methodology could easily be extended to other targeting therapies, whenever the

compounds contain heavy particle emitters or isotopes that could give rise to heavy particle emitters following irradiation.

Acknowledgements

The authors gratefully acknowledge the expert advice of Dr Rómulo L. Cabrini on tissue sectioning and of Dr Maria E. Itoiz on histological analysis. The authors are also grateful for the support of Dr Claudio Devida and his team with ICP-MS measurements.

Declaration of interest

The authors report no conflicts of interest. The authors alone are responsible for the content and writing of the paper.

References

Altieri S, Bortolussi S, Bruschi P, Fossati F, Vittor K, Nano R, Facoetti A, Chiari P, Bakeine J, Clerici A, Ferrari C, Salvucci O. 2006. Boron absorption imaging in rat lung colon adenocarcinoma metastases. J Phys: Conf Ser 41:123–126.

Amemiya K, Takahashi H, Kajimoto Y, Nakazawa M, Yanagie H, Hisa T, Eriguchi M, Nakagawa Y, Majima T, Kageji T, Sakurai Y, Kobayashi T, Konishi T, Hieda K, Yasuda N, Ogura K. 2005. High-resolution nuclear track mapping in detailed cellular histology using CR-39 with the contact microscopy technique. Radiat Meas 40:283–288.

Asbury A, Ojemann RG, Nielsen SL, Sweet WH. 1972. Neuropathologic study of fourteen cases of malignant brain tumor treated by boron-10 slow neutron capture. J Neuropathol Exp Neurol 31:278–303.

Barth RF, Vicente MG, Harling OK, Kiger WS 3rd, Riley KJ, Binns PJ, Wagner FM, Suzuki M, Aihara T, Kato I, Kawabata S. 2012. Current status of boron neutron capture therapy of high grade gliomas and recurrent head and neck cancer. Radiat Oncol 7:146.

Bortolussi S, Altieri S, Protti N, Stella S, Ballarini F, Bruschi P, Gadan MA, Thorp SI, Miller M, Pozzi ECC, Trivillin VA, Garabalino MA, Molinari AJ, Monti Hughes A, Heber EM, Itoiz ME, Aromando RF, Nigg DW, Schwint AE. 2010. ^{10}B measurement by alpha spectrometry and ^{10}B imaging by neutron autoradiography as a contribution to the understanding of BNCT radiobiology in oral cancer and liver metastases animal models. Proceedings from the 14th International Congress on Neutron Capture Therapy. 25–29 October 2010; Buenos Aires, Argentina: pp 59–62.

Chandra S, Barth RF, Haider SA, Yang W, Huo T, Shaikh AL, Kabalka GW. 2013. Biodistribution and subcellular localization of an unnatural boron-containing amino acid (cis-ABCPC) by imaging secondary ion mass spectrometry for neutron capture therapy of melanomas and gliomas. PLos ONE 8:e75377.

Chandra S, Ahmad T, Barth RF, Kabalka GW. 2014. Quantitative evaluation of boron neutron capture therapy (BNCT) drugs for boron delivery and retention at subcellular-scale resolution in human glioblastoma cells with imaging secondary ion mass spectrometry (SIMS). J Microsc 254:146–156.

Coderre JA, Turcotte JC, Riley KJ, Binns PJ, Harling OK, Kiger WS. 2003. Boron Neutron Capture Therapy: cellular targeting of high linear energy transfer radiation. Technol Cancer Res Treat 2:355–375.

Diaz A, Stelzer K, Laramore G, Wiersema R. Pharmacology studies of $Na_2{}^{10}B_{10}H_{10}$ (GB-10) in human tumor patients. Proceedings from the 10th International Congress on Neutron Capture Therapy; 8–13 September 2002. Essen, Germany. pp. 993–999.

Fleischer RL, Price P, Walker RM. 1975. Nuclear tracks in solids, 1st ed. Berkeley: University of California Press.

Hawthorne MF, Lee MW. 2003. A critical assessment of boron target compounds for boron neutron capture therapy. J Neurooncol 62: 33–45.

Heber E, Trivillin VA, Nigg D, Kreimann EL, Itoiz ME, Rebagliati RJ, Batistoni D, Schwint AE. 2004. Biodistribution of GB-10 (Na(2)(10) B10H10) compound for boron neutron capture therapy (BNCT) in an experimental model of oral cancer in the hamster cheek pouch. Arch Oral Biol 49:313–324.

Heber EM, Trivillin VA, Nigg DW, Itoiz ME, Gonzalez BN, Rebagliati RJ, Batistoni D, Kreimann EL, Schwint AE. 2006. Homogeneous boron targeting of heterogeneous tumours for boron neutron capture therapy (BNCT): Chemical analyses in the hamster cheek pouch oral cancer model. Arch Oral Biol 51:922–929.

Jain RK. 2005. Normalization of tumor vasculature: An emerging concept in antiangiogenic therapy. Science 307:58–62.

Kiger WS 3rd, Micca PL, Morris GM, Coderre JA. 2002. Boron microquantification in oral muscosa and skin following administration of a neutron capture therapy agent. Radiat Prot Dosimetry 99:409–412.

Kreimann EL, Itoiz ME, Dagrosa A, Garavaglia R, Farías S, Batistoni D, Schwint AE. 2001. The hamster cheek pouch as a model of oral cancer for boron neutron capture therapy studies: Selective delivery of boron by boronophenylalanine. Cancer Res 61:8775–8781.

Lu XQ, Kiger WS. 2009. Application of a novel microdosimetry analysis and its radiobiological implication for high-LET radiation. Radiat Res 171:646–656.

Molinari AJ, Pozzi EC, Monti Hughes A, Heber EM, Garabalino MA, Thorp SI, Miller M, Itoiz ME, Aromando RF, Nigg, DW, Quintana J, Santa Cruz GA, Trivillin VA, Schwint AE. 2011. 'Sequential' boron neutron capture therapy (BNCT): A novel approach to BNCT for the treatment of oral cancer in the hamster cheek pouch model. Radiat Res 175:463–472.

Molinari AJ, Aromando RF, Itoiz ME, Garabalino MA, Monti Hughes A, Heber EM, Pozzi EC, Nigg DW, Trivillin VA, Schwint AE. 2012. Tumor blood vessel 'normalization' improves the therapeutic efficacy of boron neutron capture therapy (BNCT) in experimental oral cancer. Radiat Res 177:59–68.

Portu A, Carpano M, Dagrosa A, Nievas S, Pozzi E, Thorp S, Cabrini R, Liberman S, Saint Martin G. 2011a. Reference systems for the determination of ^{10}B through autoradiography images: Application to a melanoma experimental model. Appl Radiat Isot 69: 1698–1701.

Portu A, Bernaola OA, Nievas S, Liberman S, Saint Martin G. 2011b. Measurement of ^{10}B concentration through autoradiography images in polycarbonate nuclear track detectors. Radiat Meas 46:1154–1159.

Portu A, Carpano M, Dagrosa A, Cabrini RL, Saint Martin G. 2013. Qualitative autoradiography with polycarbonate foils enables histological and track analyses on the same section. Biotech Histochem 88:217–221.

Schütz C, Brochhausen C, Altieri S, Bartholomew K, Bortolussi S, Enzmann F, Gabel D, Hampel G, Kirkpatrick CJ, Kratz JV, Minouchehr S, Schmidberger H, Otto G. 2011. Boron determination in liver tissue by combining quantitative Neutron Capture Radiography (QNCR) and histological analysis for BNCT treatment planning at the TRIGA Mainz. Radiat Res 176:388–396.

Solares GR and Zamenhof RG. 1995. A novel approach to the microdosimetry of neutron capture therapy. Part I. High resolution quantitative autoradiography applied to microdosimetry in neutron capture therapy. Radiat Res 144:50–58.

Sweet WH, Soloway AH, Brownell GL. 1963. Boron-slow neutron capture therapy of gliomas. Acta Radiol 1:114–121.

Trivillin VA, Heber EM, Nigg DW, Itoiz ME, Calzetta O, Blaumann H, Longhino J, Schwint AE. 2006. Therapeutic success of boron neutron capture therapy (BNCT) mediated by a chemically non-selective boron agent in an experimental model of oral cancer: A new paradigm in BNCT radiobiology. Radiat Res 166:387–396.

Wittig A, Michel J, Moss RL, Stecher-Rasmussen F, Arlinghaus HF, Bendel P, Mauri PL, Altieri S, Hilger R, Salvadori PA, Menichetti L, Zamenhof R, Sauerwein WA. 2008. Boron analysis and boron imaging in biological materials for Boron Neutron Capture Therapy (BNCT). Crit Rev Oncol Hematol 68:66–90.

Wittig A, Sauerwein WA, Coderre JA. 2000. Mechanisms of transport of p-borono-phenylalanine through the cell membrane in vitro. Radiat Res 153:173–180.

Yanagie H, Ogura K, Takagi K, Maruyama K, Matsumoto T, Sakurai Y, Skvarc J, Illic R, Kuhne G, Hisa T, Yoshizaki I, Kono K, Furuya Y, Sugiyama H, Kobayashi H, Ono K, Nakagawa K, Eriguchi M. 2004. Accumulation of boron compounds to tumor with polyethyleneglycol binding liposome by using neutron capture autoradiography. Appl Radiat Isot 61:639–646.